JOURNAL OF MATERIAL SCIENCE 31 (1996) 3707–3713

A study of combustion synthesis of Ti–Al intermetallic compounds

W. Y. YANG, G. C. WEATHERLY
Department of Materials Science and Engineering, McMaster University, Hamilton, Ontario, Canada, L8S 4L7

The mechanisms involved in the combustion synthesis of Ti–Al intermetallics have been studied by quenching partially transformed pellets to suppress the reaction prior to its completion. The reaction steps leading to the formation of $TiAl_3$, TiAl or Ti_3Al were found to be similar in all three compositions used for the study. In each case the initial product detected by X-ray diffraction was $TiAl_3$, while substantial dissolution of Ti into molten Al was found. At the same time the molten Al–Ti liquid adsorbed oxygen, and on quenching the partially transformed pellet, a glass was formed from the liquid. If the combustion synthesis process was completed, the oxygen-rich liquid decomposed, yielding a mixture of oxides and intermetallic compounds.

1. Introduction

Pioneering work in Russia 25 years ago first demonstrated that self-propagating high temperature synthesis (SHS) might be an attractive method for the production of TiAl intermetallics [1–3]. In this technique the highly exothermic nature of the reaction between Ti and Al powders is used to promote the formation of the intermetallic compound by rapidly heating one end of the sample close to the melting point of Al. The reaction, once ignited, then propagates as a wave through the sample, completing the transformation. The product of SHS is a porous solid, which can be consolidated by hot pressing to full density [4]. An alternative method, reactive sintering or reactive powder processing, where the whole compact is heated uniformly [5, 6], also depends on the exothermic nature of the process.

The factors which control the thermodynamics of the process and the kinetics of the reactions between Ti and Al in SHS have been extensively studied [7–11]. Most investigators have concluded that the initial reaction between liquid Al and solid Ti involves the formation of $TiAl_3$, in agreement with the first work on this system by Mackowiak and Shreir, who studied solid Ti in contact with molten Al in the temperature range 700–850 °C [12, 13]. As the temperature of the powder compact rises to temperatures in excess of 1000 °C, a variety of other intermetallics can form by solid state reaction, depending on the average composition of the charge prior to ignition.

Although SHS has a number of attractive processing features, e.g. simplicity of operation, near net-shape forming capability and a low thermal budget, there are unfortunately some drawbacks to making TiAl intermetallics this way. In addition to the problem of porosity noted above, the high oxygen content of the final product may embrittle the alloy [6]. There are a number of potential sources of oxygen, including physical absorption of water, hydrated aluminium oxides and the high oxygen content of the Ti powder [11].

In this study the authors have interrupted the progress of the SHS reaction by quenching partially transformed compacts having nominal target compositions of $TiAl_3$, TiAl and Ti_3Al. This technique allows us to study the sequence of intermetallic phase formation at different points in the thermal cycle of the process as a function of the starting composition of the compact. The method also sheds some light on the role played by the liquid in the pick-up of oxygen by the compact.

2. Experimental procedure

Titanium and aluminium powders (Johnson Matthey, − 325 mesh, 99 and 99.5% purity, respectively) were mixed and ball milled for one day, prior to being pressed into pellets, 12.5 mm in diameter and 25 mm in length, at a compaction pressure of 75 MPa. The nominal compositions of the samples studied were chosen to correspond to the three intermetallics, $TiAl_3$ (designated PTA3), TiAl (PTA) and Ti_3Al (PT3A). The green densities of the pellets after pressing were approximately 75%.

The pellets were loaded into a tube furnace, purged with high purity argon, and then heated at $2\,^{\circ}C\,s^{-1}$ under flowing argon until one end of the pellet ignited. The thermal cycle was measured by embedding a thermocouple into the end of the sample away from the ignition point. Typical profiles for the PTA and PT3A samples are shown in Fig. 1. A number of trial runs were done to establish that it took about 15 s after ignition for the wave front to propagate the length

0022–2461

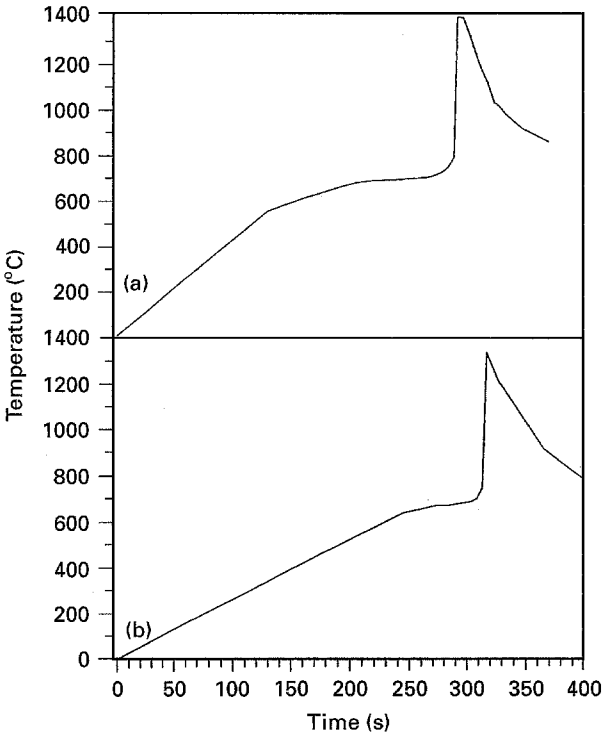

Figure 1 Temperature–time plots for samples (a) PTA and (b) PT3A, illustrating the ignition of the reaction 300 s after the start of the heating cycle, and peak reaction temperatures in excess of 1300 °C.

of the sample. Partially transformed samples were obtained by water quenching the pellets after ignition, but prior to completion of the reaction. An example of a partially reacted pellet is shown in Fig. 2.

X-ray diffraction (XRD) and transmission electron microscopy (TEM) were used to examine the phases formed at different points along the length of the partially transformed samples. Transverse slices 1 mm

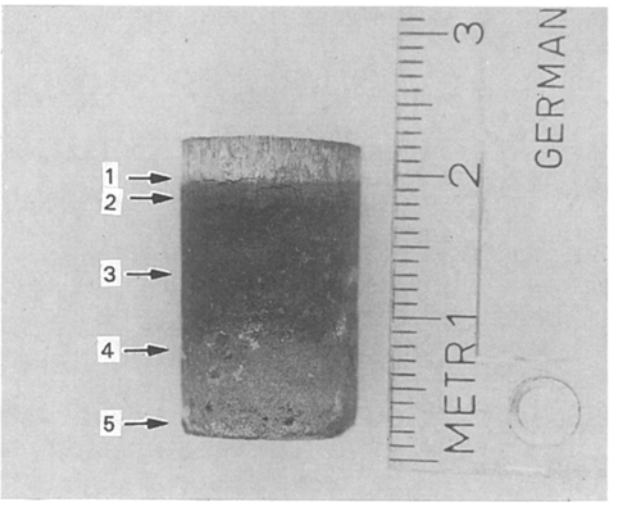

Figure 2 Partially reacted specimen showing the locations one to five from which samples were removed for analysis. The reaction was started at location five, and in this sample the wave front has just reached locations one and two prior to the quench.

thick were removed from five locations (marked 1–5 in Fig. 2) and first used for XRD measurements. The slices were then thinned for TEM by polishing to 150 μm thickness, followed by cutting 3 mm thick discs, dimple grinding to 30–40 μm and argon ion beam thinning in a Gatan Duomill. TEM was done on a Philips CM12 equipped with energy dispersive X-ray (EDX) and electron energy loss spectroscopy (EELS) facilities. EELS measurements were done using a 100 nm probe in the diffraction mode, with a convergence angle of 2.7 mrad and a collection angle of 4.1 mrad. Scanning electron microscopy (SEM) and EDX analyses were done on selected samples, prepared using standard metallographic methods on longitudinal sections.

TABLE I Summary of XRD and TEM diffraction results

		Phases detected (relative intensity in XRD analysis)					
Sample	Location	$TiAl_3$	TiAl	Ti_3Al	Ti	Al	Amorphous phase
PT3A	1	w[a]	n[b]	n	s[c]	s	n
	2	w	w	s	m[d]	w	m
	3	n	m	s	n	n	m
	4	n.d.[e]	n.d.	n.d.	n.d.	n.d.	n.d.
	5	n	w	s	n	n	n
PTA	1	w	n	n	s	s	n
	2	s	m	m	m	m	m
	3	m	s	m	w	w	m
	4	n	s	s	n	n	w
	5	n	s	m	n	n	n
PTA3	1	n.d.	n.d.	n.d.	n.d.	n.d.	n.d.
	2	s	w	n	w	s	n
	3	s	w	m	n	m	w
	4	n.d.	n.d.	n.d.	n.d.	n.d.	n.d.
	5	s	w	w	n	n	n

[a] w, weak.
[b] n, none.
[c] s, strong.
[d] m, medium.
[e] n.d., not determined.

3. Results

3.1. X-ray diffraction

The results of the XRD analysis are summarized in Table I. The first phase to form in all three samples at location one, i.e. at the leading edge of the ignition wave front shown in Fig. 2, was $TiAl_3$. For samples PT3A and PTA, this phase was no longer detected by XRD at location five, being replaced by Ti_3Al (with weak traces of TiAl) in PT3A and by TiAl (with medium traces of Ti_3Al) in PTA. (The minimum level of a phase which could be detected with the XRD set-up used in these experiments was 5%.) Since the time to propagate the wave front through the sample was estimated to be 15 s, it was concluded by inspecting Fig. 1 that the transformation to the final product was essentially complete shortly after the peak temperature of the thermal cycle was reached. An amorphous phase was detected at locations two and three in samples PT3A and PTA and at location three in sample PTA3. The preliminary identification of an amorphous phase was based on the high background detected at low scattering angles in the XRD data. An example of the behaviour of the background as a function of the sample location is shown in Fig. 3 for specimen PT3A. The presence of an amorphous phase in the quenched samples is confirmed by the TEM analysis described below.

3.2. Scanning electron microscopy

The sequence of transformations leading to the final product, demonstrated by the XRD data (Table I), was confirmed by the SEM investigation. The results from sample PTA3 are used to illustrate this point. (Similar results were obtained from samples PTA and PT3A.) In the first stage of the reaction, liquid Al reacts with Ti to form $TiAl_3$ (Fig. 4a). As the reaction proceeds, layers of the other two intermetallics, TiAl and Ti_3Al, nucleate and grow adjacent to the Ti-rich cores of the original Ti particles (Fig. 4b). For this sample the final product (Fig. 4c) consists of $TiAl_3$, with minor amounts of TiAl and Ti_3Al. However, as the volume fraction of TiAl is low only the latter is detected by EDX. The sequence of transformations is essentially the same as that found by Wang and Dahms [6], although the present authors have not detected the $TiAl_2$ phase they reported.

3.3. Transmission electron microscopy

TEM studies were used to complement the SEM results and to shed further light on the nature of the amorphous phase detected by XRD. The amorphous phase was found in all the TEM samples prepared from regions one and three of PT3A and PTA, and from region three of PTA3. Typical examples of the TEM images of this phase are shown in Fig. 5a and b, together with a representative selected area diffraction pattern displaying the diffuse ring structure of an amorphous solid. The Ti:Al atom ratios, as determined by EDX measurements, showed a wide range, from a low value of 1:7 found in an area of sample PTA3 to a high value of 15:1 in PT3A. Within any given sample broad spectra of Ti:Al values were measured in the amorphous phase; e.g. in PT3A, ratios ranging from 15:1 to 1:1 were

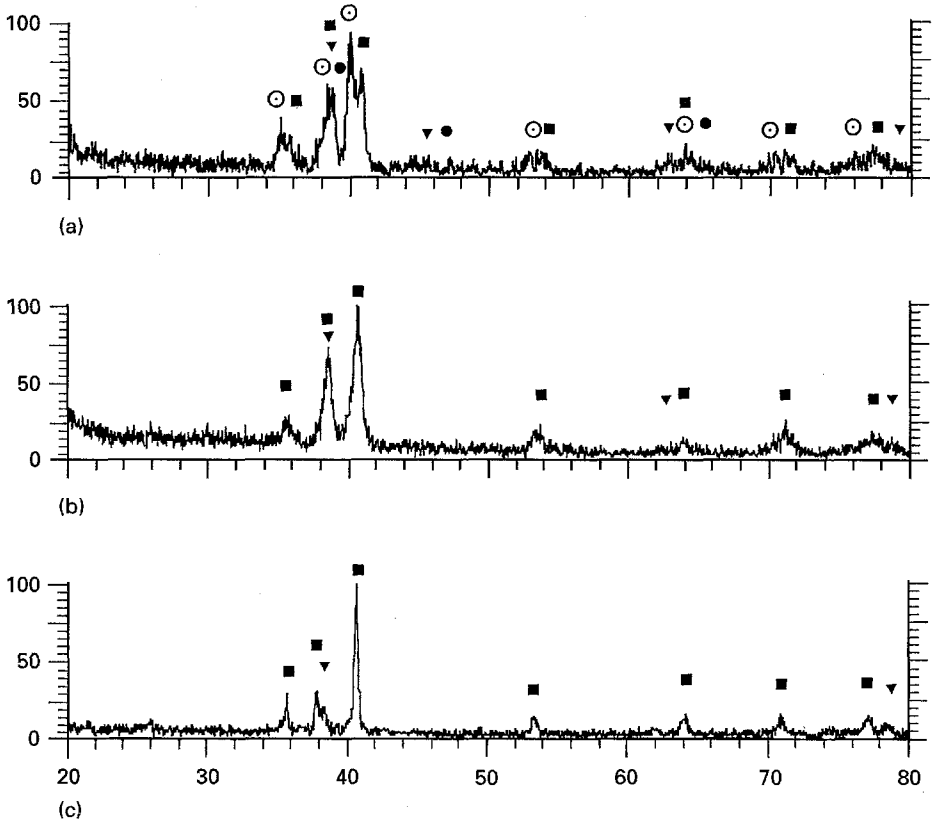

Figure 3 XRD scans of sample PT3A at locations (a) two, (b) three, and (c) five. Note the higher background (at scattering angles $< 35°$) for locations two and three, indicative of the presence of the amorphous phase. (⊙) Ti, (■) Ti_3Al, (▼) TiAl, (●) $TiAl_3$.

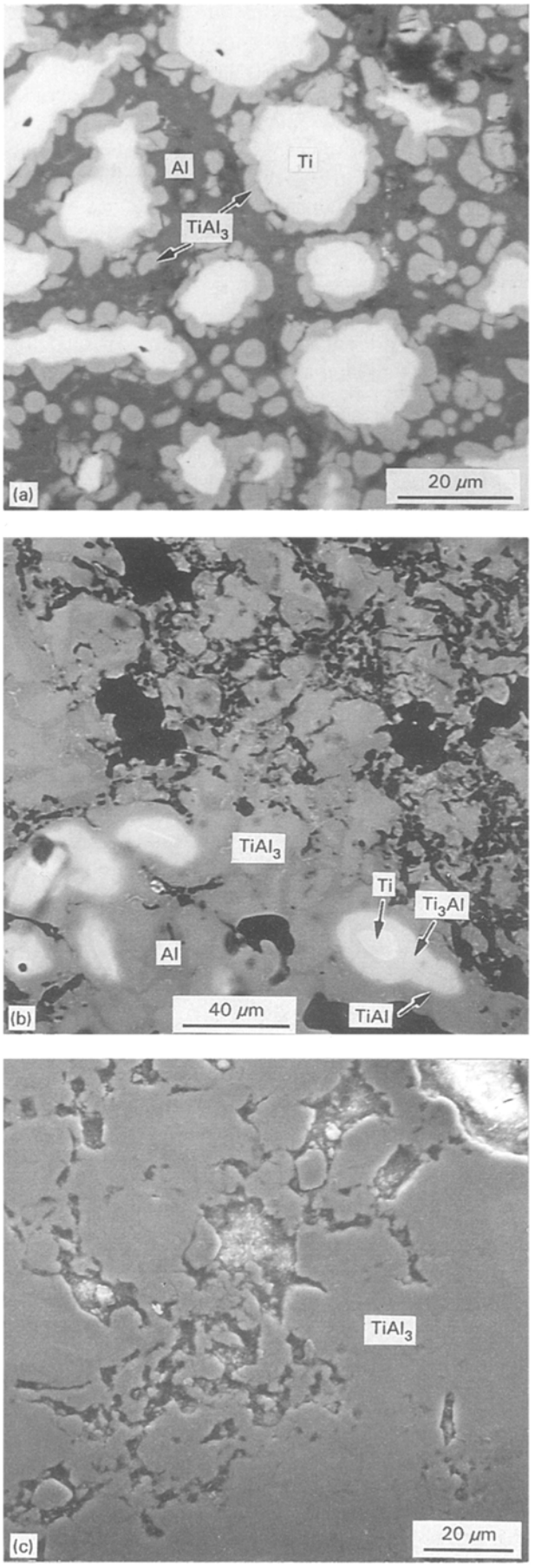

Figure 4 Sequence of SEM micrographs illustrating the progress of the reaction in sample PTA3: (a) at location one the first reaction product is $TiAl_3$; (b) locations three and four, the other intermetallics TiAl and Ti_3Al have formed (as layers) adjacent to the Ti core; and (c) location five, the reaction to $TiAl_3$ is essentially complete.

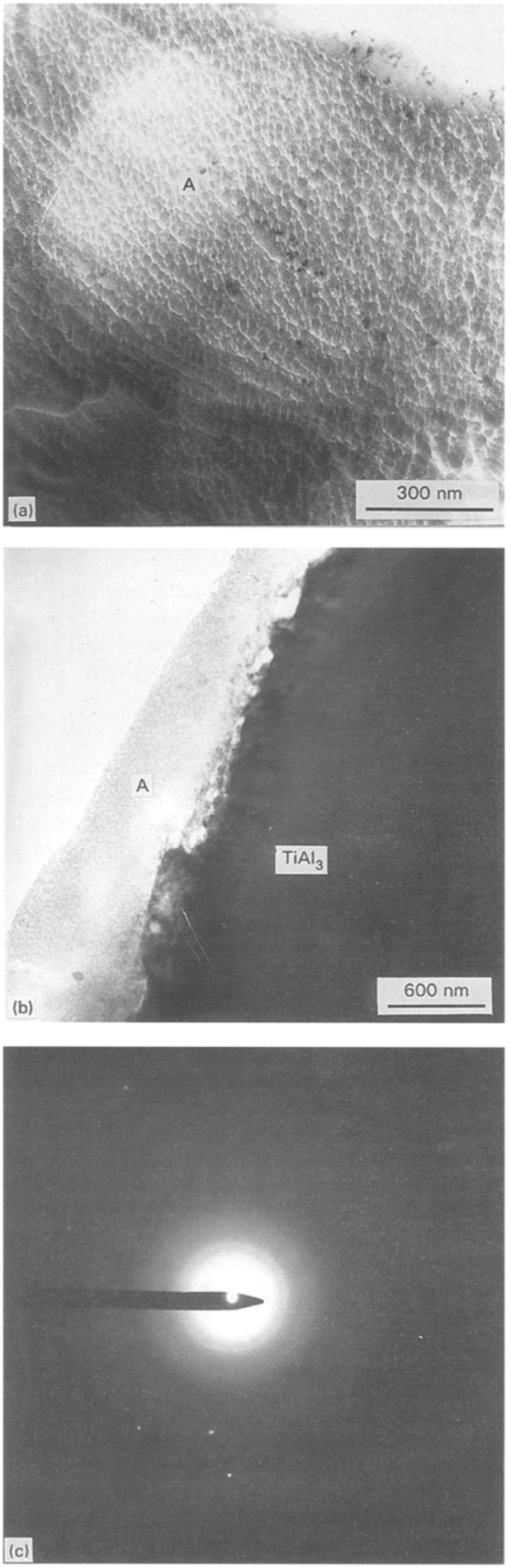

Figure 5 TEM micrographs showing the amorphous phase (A) in (a) PT3A, (b) PTA and (c) typical diffuse ring diffraction pattern from the amorphous phase.

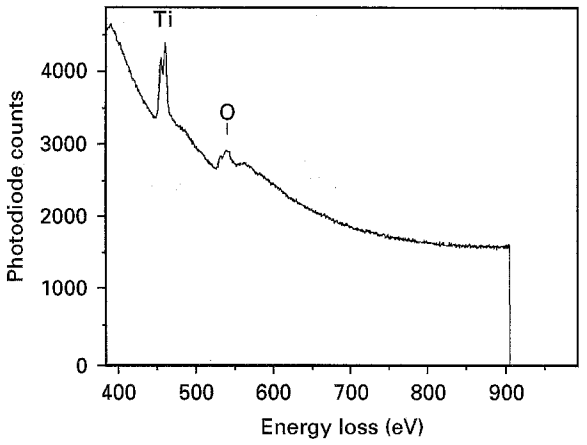

Figure 6 Electron energy loss analysis of amorphous phase in sample PT3A showing Ti and O edges.

determined. This wide range must reflect the highly non-equilibrium nature of the SHS process. The amorphous phase is stabilized by oxygen, so that on water quenching a partially reacted sample, the remaining liquid cools to form a glass rather than decomposing to crystalline phases. A rough estimate of the oxygen content of the amorphous phase was determined by running EELS measurements, following the procedures outlined earlier in the experimental section. Fig. 6 shows a typical spectrum from sample PT3A. The Ti:O atom ratio was estimated by the background subtraction procedure described in Egerton's text [14]. The Ti:O ratio for the spectrum shown in Fig. 6 was 0.3. Values ranging from 0.26 to 0.46 were determined from other areas of the same sample.

There was no evidence for an amorphous phase, from either XRD or TEM studies, at location five of any of the samples. The cooling leg of the thermal cycle of the specimens, see Fig. 1, is presumably sufficiently slow that the liquid can react with the intermetallic phases or the remaining Ti to complete the transformation. In addition to dissolving into the intermetallic compounds [6], the oxygen in the liquid can form a variety of oxide phases on cooling. The authors have not done an exhaustive search of all the oxides that might precipitate on cooling. The TEM example shown in Fig. 7a from sample PT3A, location three, illustrates fine grained oxides which have nucleated next to a region of the amorphous phase. EDX and diffraction analysis (Fig. 7b) indicate that this fine grained oxide region consists of TiO, having a rock-salt crystal structure.

The detailed analysis that can be done with the high resolution of a TEM study confirms the general picture deduced from the SEM and XRD studies for the sequence of transformations. The first phase to form by reaction of the liquid Al and solid Ti is always observed to be $TiAl_3$, irrespective of the overall composition of the sample. This is then succeeded by the formation of TiAl and finally Ti_3Al. $TiAl_3$ and Ti_3Al are always separated by a thin layer of TiAl (Fig. 8). On the other hand Ti is often found to be in direct contact with either $TiAl_3$ or TiAl (Fig. 9). No evidence is found for Ti_2Al. These observations are used in the next section to deduce the sequence of phase transformations during the thermal cycle of the SHS process.

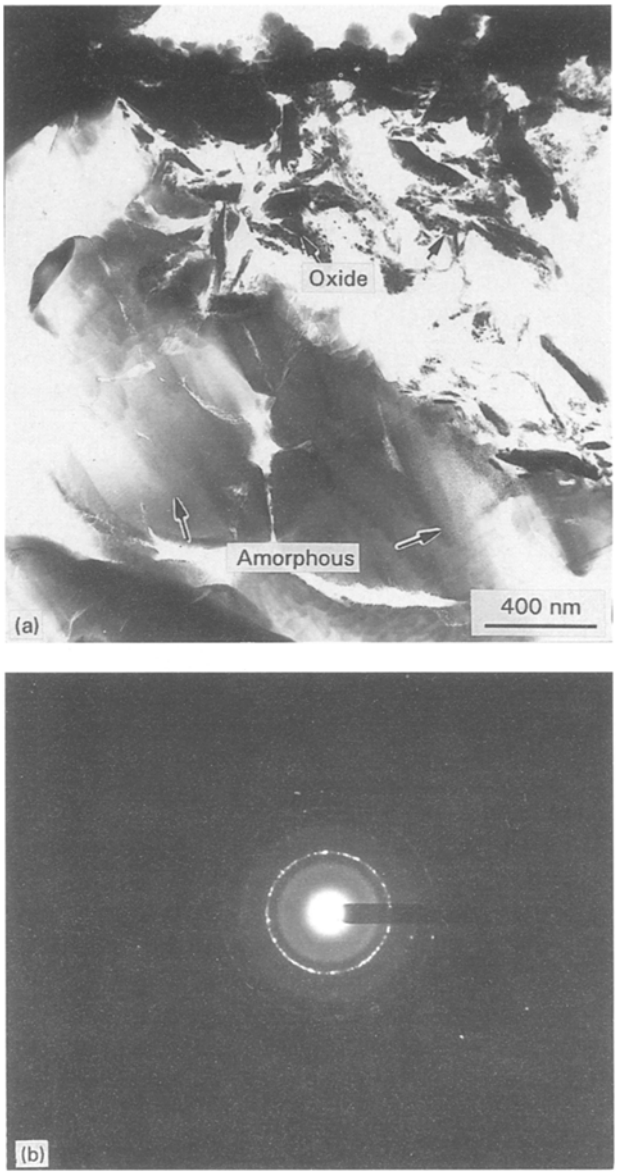

Figure 7 (a) Formation of oxides, next to an amorphous phase region, in samples PT3A. (b) Ring diffraction pattern from oxides seen in Fig. 7a, which could be analysed as cubic TiO.

4. Discussion

The kinetics of the reaction processes involved in SHS of Ti–Al intermetallics from elemental powders are rapid. The results on samples quenched from different points on the thermal cycle associated with SHS (see Fig. 1) demonstrate that the reactions are essentially complete 15 s after the ignition point. This time interval corresponds approximately to a temperature of 1200 °C on the cooling leg of the cycle, so that the temperature range of interest to SHS lies between 1200 °C and the peak temperature of the thermal cycle. The maximum temperature of 1350–1400 °C recorded by the thermocouple located at the end of the sample (see Fig. 1) probably underestimates the peak temperature of the thermal cycle in the centre of the compact. The high Ti values measured in the

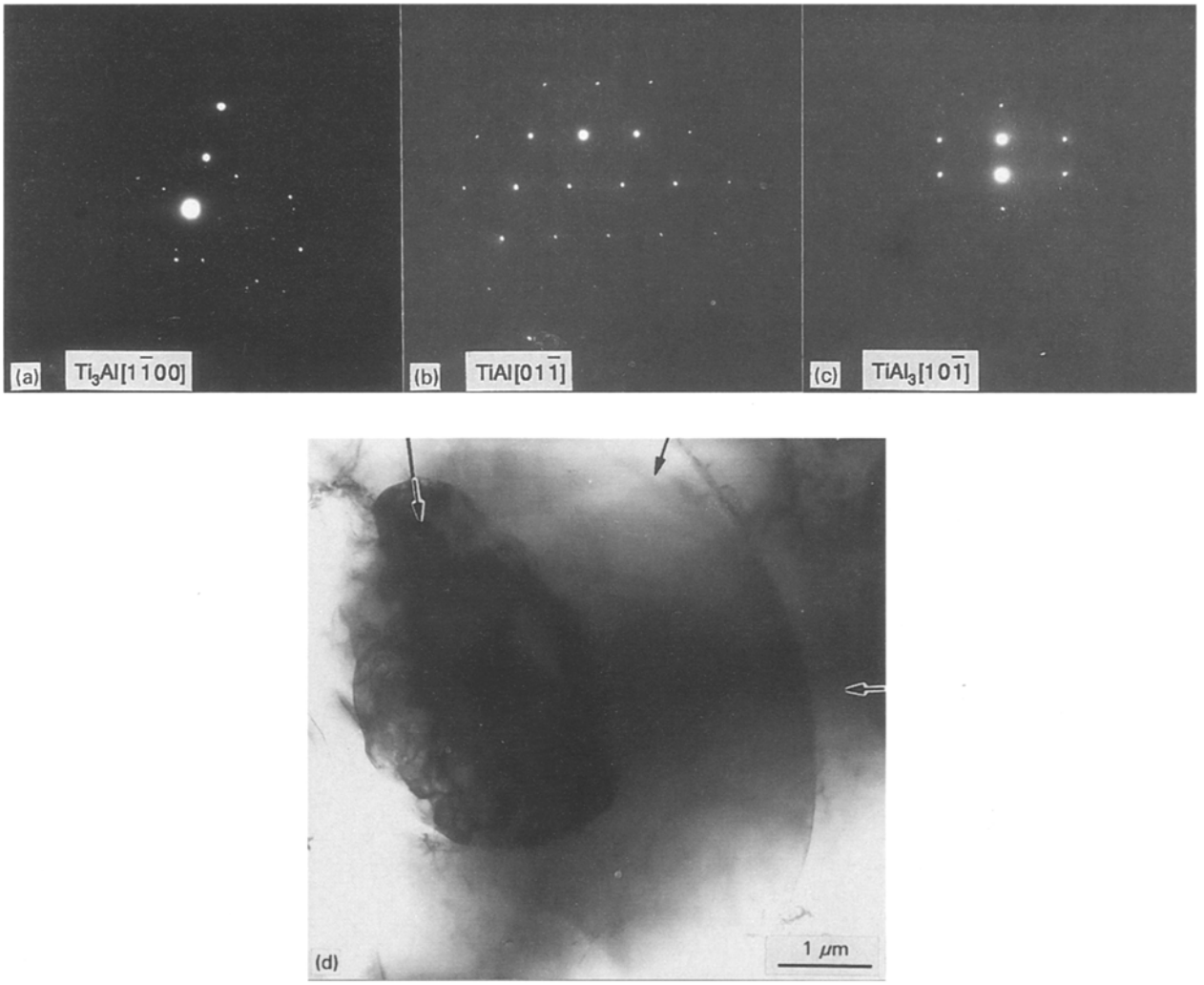

Figure 8 Electron diffraction identification of (a) Ti_3Al, (b) TiAl and (c) $TiAl_3$ in sample PTA3 (d) (compare to Fig. 4a). Note that the TiAl layer separates the Ti_3Al and $TiAl_3$ regions.

amorphous phase (Ti–Al ~ 1–15 in sample PT3A at location three) show that substantial quantities of liquid must have been present at the peak temperature. The liquidus temperatures for these compositions lie in the range of 1500–1650 °C, according to the binary Ti–Al phase diagram [15]. Further support for such high temperatures during the thermal cycle comes from a consideration of the fast kinetics observed in the formation of the intermetallics. There are no reliable solid state diffusion data for the different Ti–Al intermetallics at temperatures >1200 °C. However, if one extrapolates the diffusion data for TiAl and Ti_3Al of van Loo and Rieck [16], obtained between 700 and 1200 °C, to higher temperatures, a solid state diffusion process through an intermetallic layer could be rate controlling if temperatures in the range of 1200–1650 °C are encountered. Models of the type proposed for reactive powder processing [16], where the partially transformed powder structure is envisaged to consist of a Ti-rich core surrounded by shells of solid Ti_3Al, TiAl, etc., separating the Ti core from the liquid, can then explain the rapid kinetics of SHS.

The sequence of reactions during combustion synthesis of Ti and Al powders determined by XRD (Table I) clearly demonstrates that $TiAl_3$ is the first phase to form, irrespective of the starting composition of the compact. The heat released by the formation of $TiAl_3$ contributes to the initial rapid temperature rise after ignition. This phase, however, cannot form a barrier to further direct dissolution of Ti into Al, so that the remaining liquid becomes enriched in Ti, greatly in excess of the values that would be in equilibrium with $TiAl_3$. Indeed in the PTA and PT3A samples, $TiAl_3$ must dissolve if one is correct in suggesting that peak temperatures up to 1650 °C may exist, since $TiAl_3$ is an incongruently melting compound which dissolves at 1350 °C [15].

The presence of an amorphous phase containing a relatively high oxygen content in the quenched samples is unexpected. As noted earlier some of the oxygen may have been picked up during the quench, but undoubtedly much of it is trapped in the porous green compact and cannot be removed by argon purging. Previous studies have shown that the relatively high O content of Ti–Al intermetallics made by reactive powder processing or by SHS might limit the usefulness of these techniques [6, 11]. The range of compositions of the amorphous phase fall outside the Ti–Al–O composition where a glass might be expected to form.

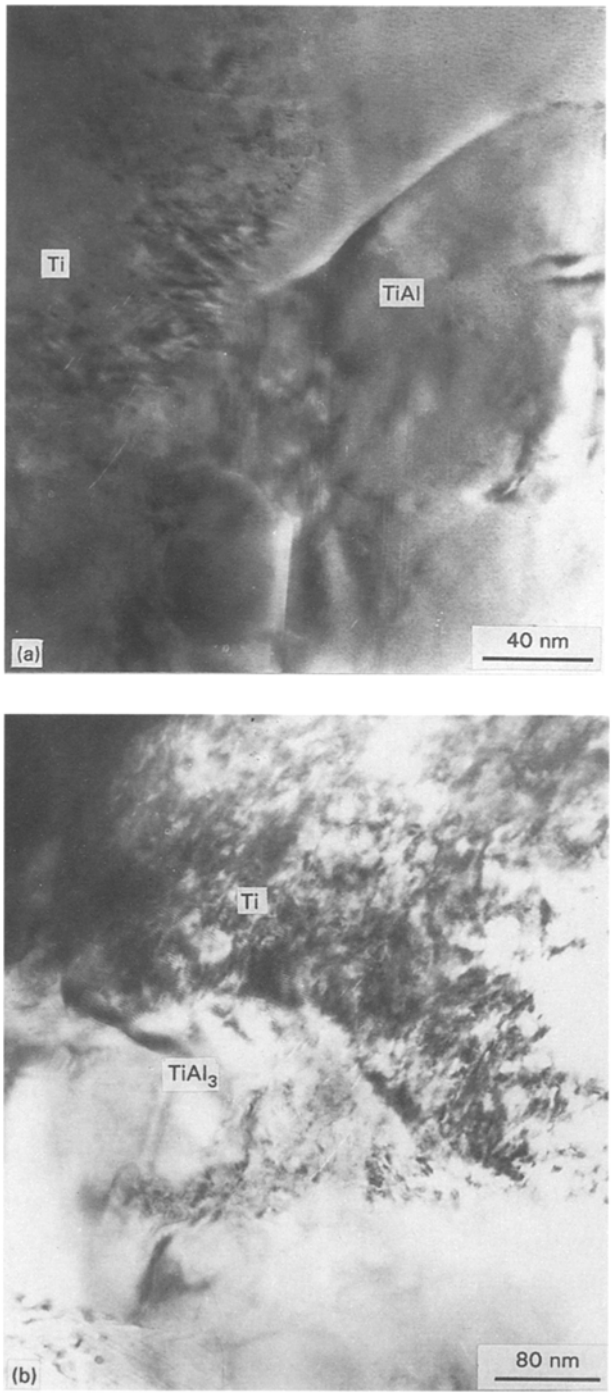

Figure 9 Areas of Ti found in direct contact with (a) TiAl, sample PTA; and (b) $TiAl_3$, sample PTA3.

The only other work where amorphous phases have been found is a recent ball-milling study of Ti and Al powder [17]. Unfortunately the O content of the powder was not reported in this study.

Acknowledgements

The authors are grateful to the Natural Sciences and Engineering Research Council of Canada for their support of this work.

References

1. A. G MERZHANOV and I. P. BOROVINSKAYA, *Dokl. Chem.* **204** (1972) 429.
2. Y. M. MAKSIMOV, A. T. PAK, G. B. LAVRENCHUK, Y. S. NAIBORENDENKO and A. G. MERZHANOV, *Comb. Explos. Shock Waves* **15** (1979) 415.
3. Y. S. NAIBORODENKO, G. B. LAVRENCHUK and V. M. FILATOV, *Soviet Powder Metall. Met. Ceram.* **21** (1982) 909.
4. Y. KAIEDA, M. NAKAMURA, M. OTAGUCHI and N. OGURU, in Proceedings of First USA–Japan Workshop on Combustion Synthesis, edited by Y. Kaieda and J. B. Holt (NRIM, Tokyo, 1990) p. 207.
5. J. C. RAWERS and W. R. WRZESINSKI, *J. Mater. Sci.* **27** (1992) 2877.
6. G. WANG and M. DAHMS, *J. Metals* **45**(5) (1993) 52.
7. A. BOSE, B. MOORE, R. M. GERMAN and N. S. STOLOFF, *ibid.* **40**(9) (1988) 14.
8. R. ODDON and R. M. GERMAN, *Adv. Powder Metall.* **3** (1989) 475.
9. J. C. RAWERS, W. R. WRZESINSKI, E. K. RAEB and R. R. BROWN, *Mater. Sci. Technol.* **6**(2) (1990) 187.
10. J. C. RAWERS and W. R. WRZESINSKI, *J. Mater. Sci.* **27** (1992) 2877.
11. H. C. YI, A. PETRIC and J. J. MOORE, *ibid.* **27** (1992) 6797.
12. J. MACKOWIAK and L. L. SHREIR, *J. Less-Common Metals* **1** (1959) 456.
13. *Idem, ibid.* **15** (1968) 341.
14. R. EGERTON, "Electron Energy Loss Spectroscopy in the Electron Microscope" (Plenum, New York, 1986).
15. T. B. MASSALSKI, H. OKAMOTO and P. R. SUBRAMANIAN (eds), "Binary Alloy Phase Diagrams", Vol. 1 (American Society for Metals, Metals Park, OH, 1986) p. 175.
16. F. J. J. VAN LOO and G. D. RIECK, *Acta Metall.* **21** (1973) 73.
17. G. J. FAN, M. X. QUAN and Z. Q. HU, *Scripta Metall. Mater.* **32** (1995) 247.

Received 28 June
and accepted 21 December 1995